International Journal of Rock Mechanics and Mining Sciences 106 (2018) 319–328

Contents lists available at ScienceDirect

International Journal of Rock Mechanics and Mining Sciences

journal homepage: www.elsevier.com/locate/ijrmms

New stability calculation method for rock slopes subject to flexural toppling failure

Guangcheng Zhang, Fei Wang*, Hu Zhang, Huiming Tang, Xianghui Li, Yuan Zhong

Faculty of Engineering, China University of Geosciences, Wuhan 430074, China

ARTICLE INFO

Keywords:
Flexural toppling
Stability factor
Tensile zone
Shear zone

ABSTRACT

Flexural toppling is one of the main failure modes of natural and manmade anti-dip layered rock slopes. Based on cantilever slab tensile theory, the failure mechanism of flexural toppling was analyzed. A toppling slope is divided into three parts: the stability, tensile and shear zones. By considering this failure mechanism, a new stability analysis method for slopes against flexural toppling failure is proposed using equilibrium theory. In addition, a sensitivity analysis is performed to investigate the locations of possible failure surfaces and zones as well as changes in the stability of anti-dip rock slopes under different conditions. The results show that the positions of the inter-column forces have almost no effect on the stability factor but affect the areas of the tensile zone and the shear zone. The angle of the most dangerous potential failure surface increases with increasing dip angle and slope height, whereas the stability factor is negatively correlated with the dip angle and slope height but is positively correlated with the layer thickness. The failure mode is essentially flexural toppling when the layer thickness is small, but the failure mode gradually transitions to shear-sliding with increasing layer thickness. Finally, a real case study is analyzed using this method, and the calculated results are consistent with the actual conditions.

1. Introduction

Toppling failures occur in rock masses containing a set of discontinuities that strike nearly parallel to the slope and dip into the slope, and these failures have been observed in both natural and manmade slopes. The term “toppling failure”, as applied to rock slopes, was first suggested by Ashby.[1] Goodman and Bray[2] summarized toppling failures as having three basic modes: flexural, block and block-flexure toppling.

Based on the limit equilibrium method, a “step-by-step” approach was proposed by Goodman and Bray[2] for the analysis of block toppling. This approach was modified by Cruden[3] and later improved by Aydan et al.[4] and Kliche.[5] Zanbak[6] constructed a set of diagrams to calculate the required support forces. Following Goodman and Bray's solution, a general analytical solution that assumes that the blocks have an infinitesimal thickness was developed.[7–9] Aydan and Kawamoto[10] first presented a theoretical method based on the limit equilibrium method and applied the bending theory of cantilever beams to analyze flexural toppling failures. Based on the principle of compatibility equations, Amini et al.[11] presented a new method for analyzing and computing the safety factor for flexural toppling failure. Amini et al.[12] presented a new analytical approach for block-flexure toppling and developed a computer code for stability analysis and assessment. Tatone BSA and Grasselli[13] developed a Monte Carlo simulation procedure for the probabilistic analysis of block toppling and described its implementation in a spreadsheet-based program (ROCKTOPPLE).

Physical and numerical modeling is also used to understand the mechanisms underlying toppling failures as well as the potential for stabilizing toppling failures. Physical modeling methods involving base friction models and tilt tables were popular in the 1970s and early 1980s. Ashby[1] utilized base friction models and tilt tables to study the slipping and toppling mechanisms acting on jointed rock slopes. Bray and Goodman[14] carried out base friction tests and analyzed the corresponding theoretical and experimental results. Recent physical modeling of rock toppling has involved centrifuge modeling. Adhikary et al.[15,16] performed a series of centrifuge experiments to investigate the mechanism of flexural toppling failure and observed the following: (1) the basal failure plane extended from the toe of the slope and was oriented at an angle of 12–20 degrees upward from the normal to the layers; and (2) the two main failure mechanisms of flexural toppling, instantaneous and progressive failure, were controlled by the magnitude of the joint friction angle. Zhang et al.[17] observed in centrifuge tests that the failure mode did not follow a straight failure plane, as was proposed by Goodman and Bray.

* Corresponding author.
E-mail address: feiwang@cug.edu.cn (F. Wang).

https://doi.org/10.1016/j.ijrmms.2018.04.016
Received 7 April 2017; Received in revised form 20 December 2017; Accepted 7 April 2018

Because physical modeling requires considerable time and large monetary costs, numerical simulation, which is an effective method, is commonly used to investigate the toppling failure mechanisms of rock slopes. Since the 1970s, many numerical techniques have been developed and successfully applied to the modeling of toppling failures. These techniques include the distinct element method (DEM)[18–20] and the universal distinct element code (UDEC).[21–23] Adhikary et al.[24–26] developed a finite element model that was based on the Cosserat theory to investigate the mechanisms of flexural toppling failure. Alzo'ubi et al.[27] used the UDEC damage model (UDEC-DM), which is a numerical modeling methodology based on a discrete element framework, to investigate two centrifuge tests carried out by Adhikary et al.[25] and Zhang et al.[17] to examine the toppling process.

As described above, many studies have been performed on toppling failures and have resulted in significant achievements. Block toppling and flexural toppling are two distinct types of toppling failure mode, and the stability analysis method proposed by Goodman and Bray[2] on block toppling is not appropriate for flexural toppling. Reference[10–12,15,16] have developed a new technique, which consider the stratified rock slopes as a series of cantilever slabs, to calculate the stability of flexural toppling. However, the mechanism of flexural toppling has not been clarified, especially the location of the failure surface. Therefore, this paper investigates the mechanisms underlying flexural toppling failure based on cantilever slab theory and the limit equilibrium method, and presents a new stability calculation method for flexural toppling failure.

2. The ultimate tensile length of a cantilever slab

Flexural toppling of stratified rock slopes can be considered to involve a series of cantilever slabs and the interacting forces between the adjacent slabs; a geomechanical model of this is shown in Fig. 1. Under the influence of external forces, these cantilever slabs deform and even fail via tensile or shear failure modes. According to the stability and failure mechanisms, a rock slope subject to flexural toppling is divided into three parts from the crest to the toe: the stability zone, the tensile zone and the shear zone. Furthermore, the tensile zone forms earlier than the shear zone. Employing the column theory from the theory of elasticity, the absolute value of the minimum normal stress σ_x at the base of a column with unit thickness is given as follows:

$$\sigma_x = \frac{M}{I}y - \frac{N}{A} \tag{1}$$

where y denotes the thickness of the column (m), N denotes the normal force (kN), M denotes the moment (kN m), I denotes the inertia modulus (m^4), and A denotes the cross-sectional area of the column (m^2).

For a cantilever slab with a base inclination of β that is acted on by gravity, Eq. (1) takes the following explicit form:

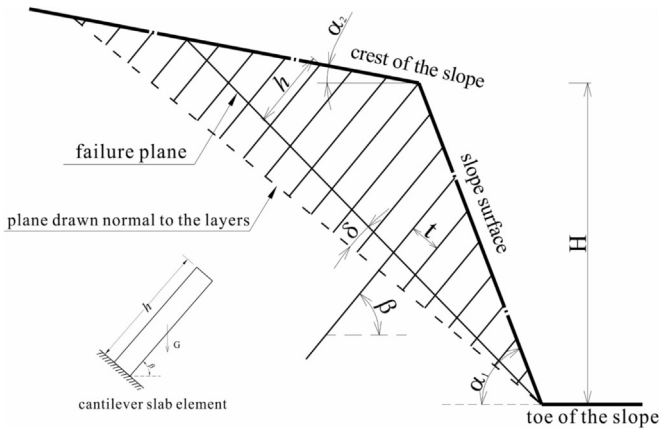

Fig. 1. Geomechanical model for flexural toppling failure of rock slopes.

$$\sigma_x = \frac{3\gamma h^2 \cos\beta}{t} - \gamma h \sin\beta \tag{2}$$

where γ denotes the unit weight of the column (kN), h denotes the column height (m), and t denotes the column thickness. In the tensile zone, every cantilever experiences tensile damage at the base of the column. Considering the stability factor k, the ultimate condition is expressed as follows:

$$\sigma_x = \frac{\sigma_t}{k} \tag{3}$$

where σ_t denotes the tensile strength of the column. By combining Eqs. (2) and (3), we obtain the limiting tensile length of the column $h_{\lim}$ under gravity:

$$h_{\lim} = \frac{t}{6}\tan\beta + \frac{1}{6}\sqrt{(t\tan\beta)^2 + 12\frac{[\sigma_t]t}{\gamma k\cos\beta}} \tag{4}$$

3. Failure mechanism of flexural toppling

Assuming that any one column of the toppling rock slope is first damaged by tension, its length should be longer than the limiting tensile length calculated using Eq. (4). This column then produces a flexural deformation larger than that of the upper column, which fails further due to tension if this column is also longer than the limiting tensile length. In this way, all columns with lengths that are not less than the limiting tensile length above the first column that was damaged by tension also fail due to tension. Then, the column above the top column that is damaged by tension deforms and separates from the overlying and underlying columns. There are no interactive forces between this column and the two adjacent columns, which is also true for all columns above the column with the limiting tensile length. Therefore, this column does not fail due to gravity only. In conclusion, the column with the limiting tensile length above the tensile zone is the lower boundary of the stability zone.

As shown above, all the columns experiencing tensile failure above the first column that failed in tension make up a retrogressive failure. The column immediately below the first column that experienced tensile failure due to gravity and the driving force is very likely to be damaged by tension; that is, the size of the tensile zone gradually increases until the normal stress is less than the tensile strength of the base of the column. This tensile region below the first column that experienced tensile failure is a push failure. Therefore, the tensile zone is divided into two subzones. The column length at the lower boundary of the tensile zone is denoted by h_x. The region between the lower boundary of the tensile zone and the toe of the slope is the shear zone. Based on this discussion, the failure mode of rock slopes that experience flexural toppling is described in Fig. 2. Furthermore, the size of each zone along the failure surface is expressed as shown in Fig. 2 and calculated using the following equations.

First, the length of the failure surface behind the base of the longest column, l_{down}, and the length of the failure surface ahead of the base of the longest column, l_{up}, are calculated as follows:

$$\begin{aligned} l_{down} &= -y_{\max}\tan(\alpha_1 + \beta) \\ l_{up} &= y_{\max}\tan(\alpha_2 + \beta) \end{aligned} \tag{5}$$

where y_{max} indicates the length of the column at the top of the rock slope, which can be obtained as follows:

$$y_{\max} = -\frac{\cos(\alpha_1 + \beta)}{\sin\alpha_1}H \tag{6}$$

Based on the geometric relationships, we obtain the following equations:

$$h_{\lim} = y_{\lim} - \Delta y_{\lim} = \frac{l_{up} + x_{\lim}}{l_{up}}y_{\max} - (l_{down} - x_{\lim})\tan\delta \tag{7}$$

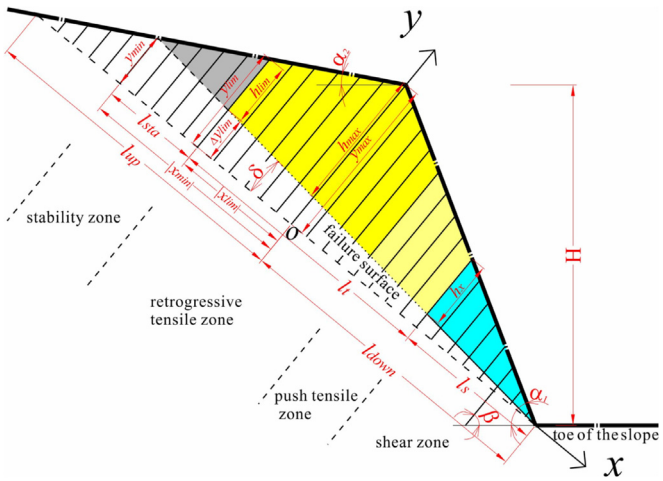

Fig. 2. Failure mechanism of flexural toppling on rock slopes.

$$\tan(90-\alpha_2-\beta)=\frac{y_{\min}}{l_{up}+x_{\min}} \tag{8a}$$

$$\tan\delta=\frac{y_{\min}}{l_{down}-x_{\min}} \tag{8b}$$

where x_{lim} and x_{min} denote the x-coordinates of the column with the limiting tensile length and the intersection point between the failure plane and solid ground, respectively.

Based on Eq. (7), x_{lim} is written as follows:

$$x_{\lim}=\frac{h_{\lim}-y_{\max}+l_{down}\tan\delta}{(\tan\delta+\frac{y_{\max}}{l_{up}})} \tag{9}$$

By combining Eq. (8a) and Eq. (8b), we obtain x_{min} as follows:

$$x_{\min}=\frac{\tan(\alpha_2+\beta)l_{up}+\tan\delta l_{down}}{\tan\delta-\tan(\alpha_2+\beta)} \tag{10}$$

Then, the length of the failure surface in the stability zone l_{sta} is calculated as follows:

$$l_{sta}=x_{\lim}-x_{\min} \tag{11}$$

Using x, which is the x-coordinate of the boundary between the tensile zone and the shear zone, the lengths of the failure surfaces in the tensile zone, l_t, and the shear zone, l_s, are expressed as follows:

$$\begin{aligned} &y=(l_{up}+x)\tan(90-\alpha_2-\beta)\\ &l_{t,down}=0\\ &l_s=l_{down}-x\\ &l_{t,up}=x-x_{\lim} \end{aligned}\qquad (x\le 0) \tag{12a}$$

$$\begin{aligned} &y=l_s\tan(\alpha_1+\beta-90)\\ &l_{t,down}=x\\ &l_s=l_{down}-x\\ &l_{t,up}=-x_{\lim} \end{aligned}\qquad (x>0) \tag{12b}$$

where $l_{t,down}$ denotes the length of the failure surface in the tensile zone in the lower portion of this region, and $l_{t,up}$ denotes the length of the failure surface in the tensile zone in the upper portion of this region. Furthermore, the area and weight of the tensile zone and the shear zone are obtained as follows:

$$\begin{aligned} &G_{t,up}=\tfrac{\gamma}{2}(h_{\lim}+h_x)(x-x_{\lim})\\ &G_{t,down}=0\\ &G_s=\tfrac{\gamma}{2}[h_{max}l_{down}-(h_x+h_{max})x] \end{aligned} \tag{13a}$$

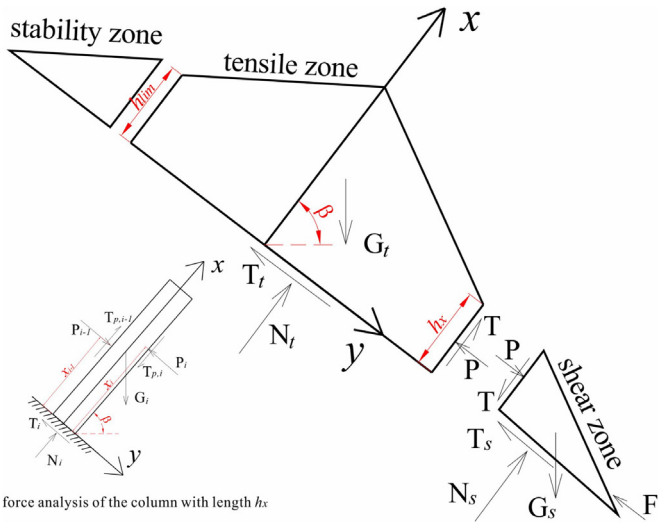

Fig. 3. Force analyses of the tensile zone and the shear zone within a flexural toppling failure.

$$\begin{aligned} &G_{t,up}=\tfrac{\gamma}{2}(h_{\lim}+h_{\max})(-x_{\lim})\\ &G_{t,down}=\tfrac{\gamma}{2}(h_x+h_{\max})x\\ &G_s=\tfrac{\gamma}{2}h_x(l_{down}-x) \end{aligned} \tag{13b}$$

where $G_{t,up}$, $G_{t,down}$ and G_s denote the weights of the tensile zone above the longest column (kN), the tensile zone below the longest column (kN), and the shear zone (kN), respectively.

4. Stability calculation method for flexural toppling failure

The stability factor is an important index for evaluating the degree of stability of slopes, and its accuracy could be increased by considering the slope failure mechanism. Based on the failure mechanism analysis of rock slopes that experience flexural toppling described above, a stability factor calculation method is proposed that uses the limit equilibrium theory. Fig. 3 shows the force system of the tensile zone and the shear zone of a flexural toppling failure under the effects of gravity without considering water, earthquakes, or other factors.

This analysis assumes that the Mohr-Coulomb criterion is obeyed on the failure surface of the tensile zone after a tensile failure occurs, on the failure surface in the shear zone, and on the contact between these two zones.

For tensile failure in hard strata, the rupture surface should be normal to the layer. Thus, the failure surface in the tensile zone is not planar; it should have the shape shown in Fig. 4(b). In this paper, we assume that failure surfaces with this shape follow the “two-plane model”. This model differs from the “one-plane model” shown in Fig. 4(a), which is usually applicable to relatively soft strata, in which the failure surface is planar.

The equations of static equilibrium can be obtained in the tensile zones of both the one-plane model and the two-plane model. Mode I is reflected by the following:

$$\begin{aligned} &N_t\cos\delta+\frac{N_t\tan\varphi_t+c_tl_t/\cos\delta}{k}\sin\delta+\frac{P\tan\varphi+ch_x}{k}=G_t\sin\beta\\ &P+\frac{N_t\tan\varphi_t+c_tl_t/\cos\delta}{k}\cos\delta=N_t\sin\delta+G_t\cos\beta \end{aligned} \tag{14a}$$

and Mode II is reflected by the following:

$$\begin{aligned} &N_t+\frac{P\tan\varphi+ch_x}{k}=G_t\sin\beta\\ &P+\frac{N_t\tan\varphi_t+c_tl_t}{k}=G_t\cos\beta \end{aligned} \tag{14b}$$

where N_t denotes the normal force at the base of the tensile zone (kN); P denotes the normal force on the contact between the tensile zone and

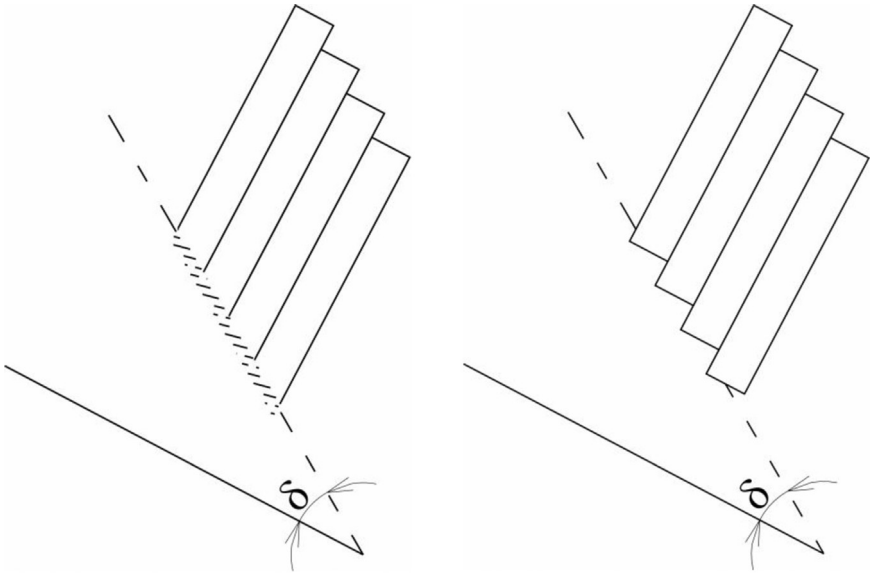

(a) Model Ⅰ (b) Model Ⅱ

Fig. 4. Failure surface model of flexural toppling failure.

	A	B	C	D	E	F	G	H	I	J	T	V	Y
1	slope angle α	crest angle θ	sliding surface δ	inclintion of layer β	slope height H	thickness t	x_p/h_s	x_{limit}	y_{limit}	y_{max}	failure plane model		
2	80	0	9.801621024	55	8.5	0.35	0.50	-3.10	3.93	6.10	1		
3	γ(kN/m³)	C(kPa)	φ	Cs(kPa)	φ_s	C_r(kPa)	φ_r	σ_t(MPa)	Δy_{limit}	Δy_{max}	1--Model I		
4	23.00	0.00	10.00	98.00	34.80	75.00	28.10	2.300	1.59	1.05	0--Model II		
5	N_{up}	N_{down}	l_{up}	l_{down}	x_{min}	Δy_{min}	y for toppling	K	h_{limit}	h_{max}	Necessary Conditions		
6	17	18	8.72	6.10	-5.78	2.05	0.50	**2.285**	2.34	5.05	>=0	>=0	>1
7	No.	x	y	Δy	l_s	$l_{t,up}$	$l_{t,down}$	l_s	G_t	G_s	P(kN)	F(kN)	σt/[σt]
9	35	-5.78	2.05	2.05	11.89	0.00	0.00	11.89	0.00	690.14	0.00	-173.48	0.00
10	34	-5.44	2.29	1.99							0.00	-159.75	0.00
11	33	-5.10	2.53	1.94							0.00	-147.12	0.03
12	32	-4.76	2.77	1.88							0.00	-135.58	0.07
13	31	-4.42	3.01	1.82							0.00	-125.14	0.14
14	30	-4.08	3.24	1.76							0.00	-115.80	0.22
15	29	-3.74	3.48	1.70							0.00	-107.54	0.32
16	28	-3.40	3.72	1.64							0.00	-100.39	0.45
17	27	-3.06	3.96	1.58							-0.14	-94.47	0.60
18	26	-2.72	4.20	1.52							-0.82	-90.17	0.80
19	25	-2.38	4.44	1.47							-0.26	-85.75	0.90
20	24	-2.04	4.67	1.41							1.52	-81.22	1.00
21	23	-1.70	4.91	1.35							4.53	-76.56	1.09
22	22	-1.36	5.15	1.29							8.76	-71.78	1.17
23	21	-1.02	5.39	1.23							14.22	-66.88	1.25
24	20	-0.68	5.63	1.17							20.91	-61.86	1.32
25	19	-0.34	5.86	1.11							28.83	-56.73	1.38
26	18	0.00	6.10	1.05							37.97	-51.47	1.44
27	17	0.34	5.76	1.00							47.12	-46.23	1.66
28	16	0.68	5.43	0.94							55.11	-41.10	1.63
29	15	1.02	5.09	0.88							61.94	-36.08	1.58
30	14	1.36	4.75	0.82							67.62	-31.17	1.54
31	13	1.70	4.41	0.76							72.15	-26.38	1.48
32	12	2.03	4.07	0.70							75.52	-21.70	1.43
33	11	2.37	3.73	0.64							77.74	-17.14	1.36
34	10	2.71	3.39	0.59							78.80	-12.68	1.29
35	9	3.05	3.05	0.53							78.71	-8.34	1.21
36	8	3.39	2.71	0.47	2.71	3.10	3.39	2.71	547.75	70.00	77.46	-4.11	1.13
37	7	3.73	2.37	0.41	2.37	3.10	3.73	2.37	564.15	53.59	75.05	0.00	1.04
38	6	4.07	2.03	0.35	2.03	3.10	4.07	2.03	578.37	39.37	71.50	4.00	0.95
39	5	4.41	1.70	0.29	1.70	3.10	4.41	1.70	590.40	27.34	66.78	7.89	0.84
40	4	4.75	1.36	0.23	1.36	3.10	4.75	1.36	600.24	17.50	60.91	11.67	0.74
41	3	5.09	1.02	0.18	1.02	3.10	5.09	1.02	607.90	9.84	53.89	15.33	0.62
42	2	5.43	0.68	0.12	0.68	3.10	5.43	0.68	613.37	4.37	45.71	18.88	0.51
43	1	5.76	0.34	0.06	0.34	3.10	5.76	0.34	616.65	1.09	36.38	22.32	0.38

Fig. 5. Microsoft Excel spreadsheet for performing the calculations in the proposed method.

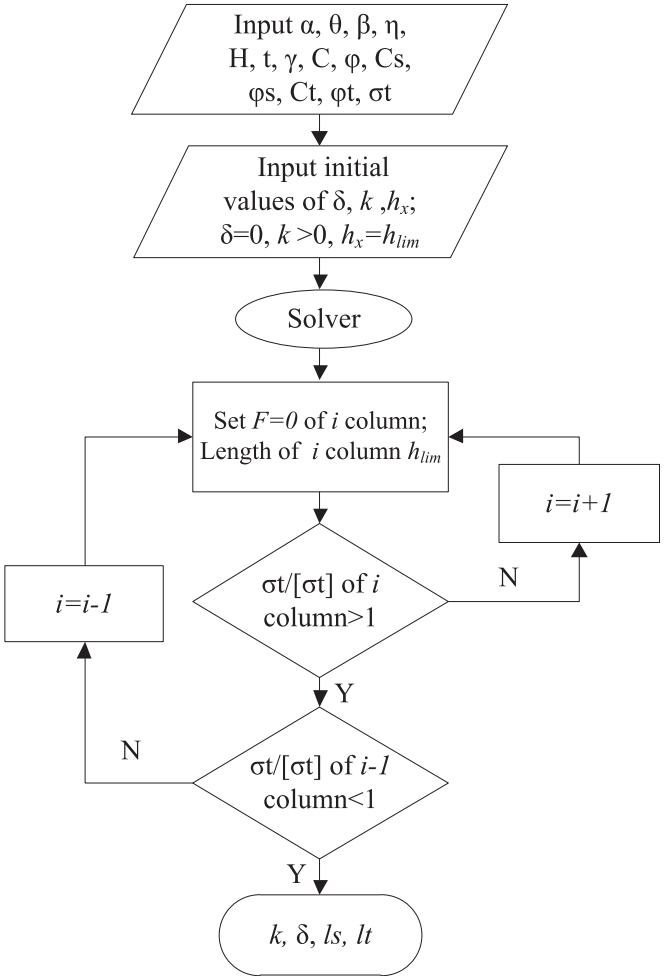

Fig. 6. Flow chart of the computational process.

the shear zone (kN); G_t denotes the weight of the tensile zone (kN); c (kPa) and φ (°) denote the cohesion and friction angle of the interlayer, respectively; and c_t (kPa) and φ_t (°) denote the cohesion and friction angle of the residual shear strength of the column, respectively.

The following equations for Mode I and Mode II are then deduced as shown in Eq. (15a) and Eq. (15b), respectively:

$$N_t = \frac{k^2 G_t \sin\beta - kc_t l_t \tan\delta - kG_t \cos\beta \tan\varphi + c_t l_t \tan\varphi - kch_x}{k^2 \cos\delta + k \sin\delta(\tan\varphi_t + \tan\varphi) - \cos\delta \tan\varphi_t \tan\varphi}$$
$$P = G_t \cos\beta + \left(\sin\delta - \frac{\tan\varphi_t}{k}\cos\delta\right)N_t - \frac{c_t l_t}{k} \quad (15a)$$

$$N_t = \frac{k^2 G_t \sin\beta - kG_t \cos\beta \tan\varphi + c_t l_t \tan\varphi - kch_x}{k^2 - \tan\varphi_t \tan\varphi}$$
$$P = G_t \cos\beta - \frac{N_t \tan\varphi_t + c_t l_t}{k} \quad (15b)$$

In the shear zone, the equations of static equilibrium are obtained as follows:

$$N_s \cos\delta + \frac{N_s \tan\varphi_s + c_s l_s / \cos\delta}{k}\sin\delta = \frac{P\tan\varphi + ch_x}{k} + G_s \sin\beta$$
$$N_s sin\delta + P + G_s \cos\beta = F + \frac{N_s \tan\varphi_s + c_s l_s / \cos\delta}{k}\cos\delta \quad (16)$$

where N_s denotes the normal force at the base of the shear zone (kN); G_s denotes the weight of the shear zone (kN); F is an assumed force at the toe of the slope (kN) that operates parallel to the failure plane; and c_s (kPa) and φ_s (°) denote the cohesion and frictional angle of the peak shear strength of the column, respectively.

Thus, we obtain the following equations:

$$N_s = \frac{P\tan\varphi + ch_x + kG_s \sin\beta - c_s l_s \tan\delta}{\tan\varphi_s \sin\delta + k\cos\delta}$$
$$F = P - \left(\frac{\tan\varphi_s}{k}\cos\delta - sin\delta\right)N_s - \frac{c_s l_s}{k} + G_s \cos\beta \quad (17)$$

The normal force operating on the contact between the two zones and the assumed force are obtained by combining Eqs. (15) and (17).

The parameters k and h_x are two key quantities that must be calculated. However, they can be determined by the trial method. Given initial values of k and h_x, F is calculated. There is inevitably a value of k that makes F equal to zero; this value of k is the actual stability factor of the rock slope.

Different stability factors are obtained using different values of h_x. Therefore, the true value of h_x should be determined. Here, we assumed that the initial value of h_x is equal to h_{lim}. We then obtain the stability factor using the Solver tool in Microsoft Excel by setting F equal to zero. Furthermore, P, N_t and N_s are obtained using Eqs. (15) and (17). However, we should determine whether there is damage due to tension at the position of the column with length h_x. For this column, the following formula is obtained by employing the column theory from the theory of elasticity:

$$\sigma_{h_x} = \frac{M}{I}y - \frac{G_i \sin\beta + T_{i-1} - T_i}{t} \quad (18)$$

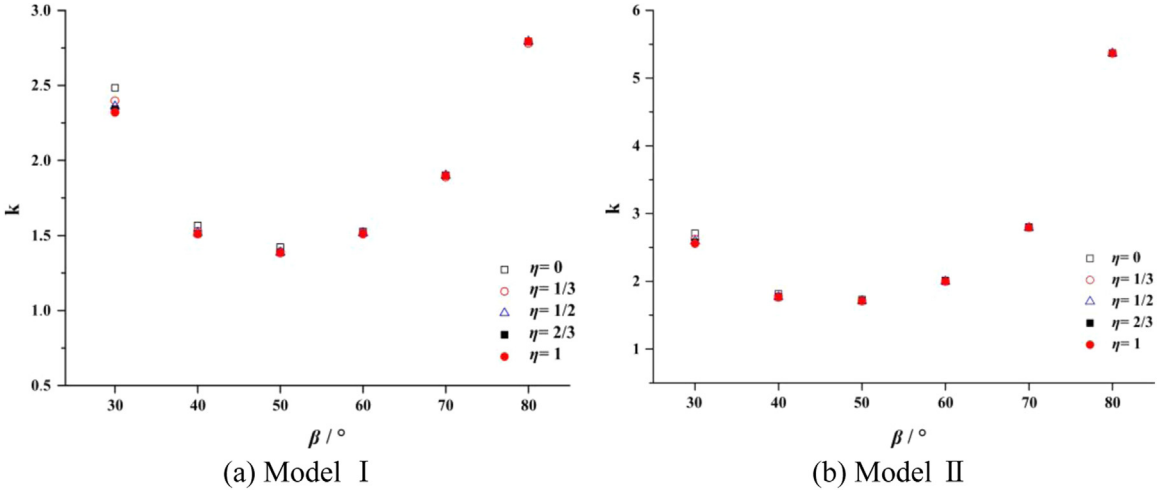

Fig. 7. The stability factor, k, as a function of the layer inclination (H = 17 m, t = 0.1 m, δ = 9°).

Table 1
Properties of the rock slope and rock mass.

	Geometric parameters		Physical properties	Shear strength						Tensile strength
	Slope angle (°)	Crest angle (°)	Density (gr/cm^3)	Shear zone		Tensile zone		Structural plane		σ_t (MPa)
				c_s (kPa)	φ_s (°)	c_t (kPa)	φ_t (°)	c (kPa)	φ (°)	
Amini et al.	80	0	2.3	98	34.8	75	28.1	/	/	2.3
Linda landslide	35	− 15	2.7	200	38	70	27	150	20	12

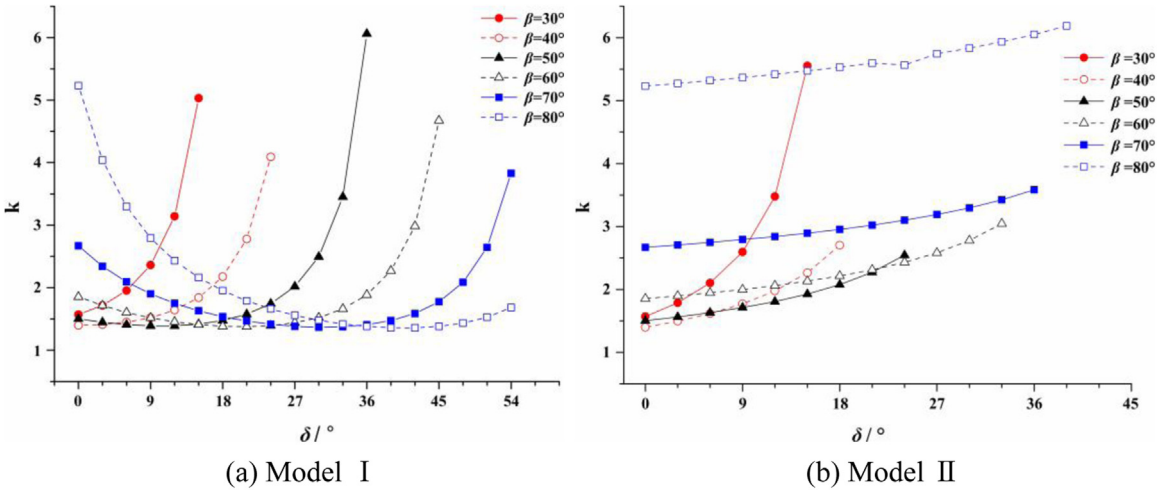

Fig. 8. The stability factor, k, as a function of δ and β (H = 17 m, t = 0.1 m, η = 0.5).

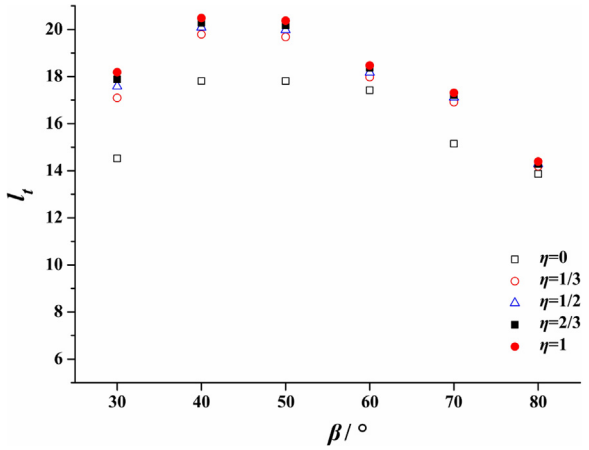

Fig. 9. Length of the failure surface in the tensile zone, l_t, as a function of the layer inclination.

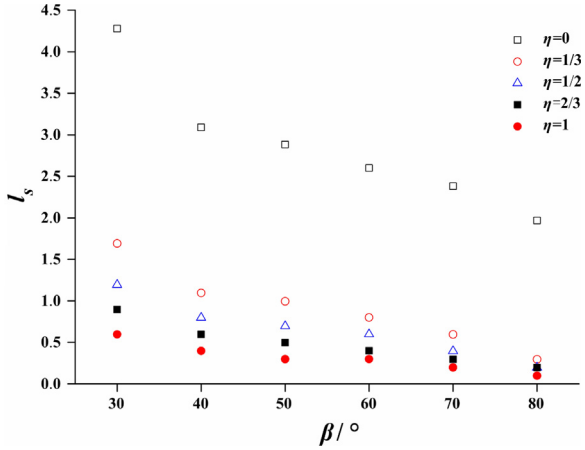

Fig. 10. Length of the failure surface in the shear zone, l_s, as a function of the layer inclination.

where T_{i-1} and T_i denote the tangential force of the contact interlayers above and below the column with length h_x, respectively; and G_i denotes the weight of the column with length h_x. The necessary condition for tensile failure of the column with length h_x is calculated using the following expression:

$$\frac{6(P_{i-1}x_{i-1} - P_i x_i) + 3G_i \cos\beta h_{i,x}}{t^2} - \frac{G_i \sin\beta + T_{i-1} - T_i}{t} \begin{cases} \geq \frac{\sigma_t}{k} & (\textit{tensile failure}) \quad (19a) \\ < \frac{\sigma_t}{k} & (\textit{shear failure}) \quad (19b) \end{cases}$$

where,

$$T_{i-1} = \frac{P_{i-1}\tan\varphi + ch_{i-1,x}}{k}$$
$$T_i = \frac{P_i \tan\varphi + ch_{i,x}}{k} \quad (20)$$

and where P_{i-1} and P_i denote the normal force on the contact interlayers above and below the column with length h_x, respectively; and x_{i-1} and x_i denote the moment arm lengths of the contact interlayers above and below point O, respectively, as shown in Fig. 3. According to Eq. (12), if the column with length h_x is determined to be experiencing tensile failure, the lower boundary of the tensile zone is moved downward; alternatively, the lower boundary should be moved upward. The actual value of h_x should satisfy Eq. (19a), and the column immediately below should satisfy Eq. (19b), which can be calculated using the trial method. The moment arm lengths in Eq. (19) are deduced

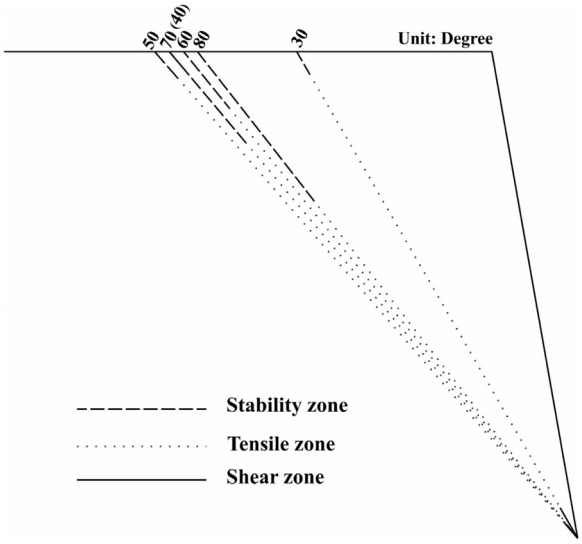

Fig. 11. Distribution of the tensile zone and the shear zone as a function of the layer inclination.

Table 2
Minimum stability factor, k, as a function of slope height and dip angle.

h	β					
	30°	40°	50°	60°	70°	80°
8.5	3.525 (0°[a])	2.471 (0°)	2.311 (6°)	2.247 (15°)	2.183 (24°)	2.084 (36°)
17.0	1.629 (0°)	1.404 (0°)	1.381 (9°)	1.359 (21°)	1.332 (30°)	1.304 (42°)
25.5	1.167 (0°)	1.075 (3°)	1.066 (12°)	1.054 (24°)	1.037 (33°)	1.027 (42°)

[a] Denotes the value of δ.

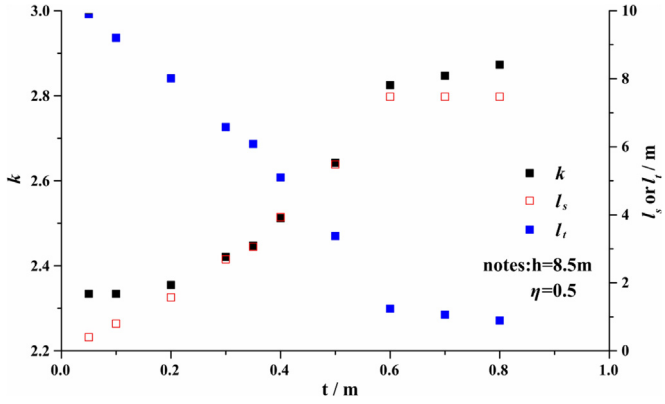

Fig. 12. Values of k, l_t and l_s as a function of the layer thickness.

using the moment balance at point O.

The position that the normal force is applied to the interlayer due to gravity is given in the following general form:

$$x_i = \eta h_{i,x} \tag{21}$$

where η is between 0 and 1. If η is known, we determine the failure mode of the i^{th} column using Eq. (19), which then determines the boundary between the tensile zone and the shear zone. Furthermore, the stability factor of flexural toppling is calculated using Eq. (17).

The analysis presented above demonstrates that the proposed stability method calculates the stability factor of rock slopes experiencing flexural toppling, and it can also determine the ranges of the stability zone, tensile zone and shear zone. Moreover, we implemented a computational program in a Microsoft Excel spreadsheet with the Solver tool, as shown in Fig. 5, and the flow chart of the process is shown in Fig. 6.

5. Sensitivity analysis of toppling rock slope stability

Using the proposed method, several studies were performed to determine the effects of different slope structures, which are expressed in terms of their inclination, layer thickness, and slope height, on the slope stability and failure surface lengths in the tensile zone and the shear zone; the results are shown in Figs. 7–12. The geometric parameters of the rock slope as well as the physical and mechanical parameters of the rock mass are shown in Table 1 based on the values from Amini et al.[28].

Fig. 7 shows that the stability factors and dip angles of the layers in both Model Iand model IIapproximately follow a second-order polynomial. The stability factor initially decreases and then increases with increasing dip angle, and the position of the force operating on the contact between the tensile zone and shear zone has a minimal impact on the stability factor. Furthermore, the minimum value of the stability factor occurs at a dip angle of 50° under these conditions.

Fig. 8 shows the variation in the stability factor using different values of δ and β for Models I and II. Fig. 8(a) shows that in Model I, when the dip angle is 30° or 40°, the minimum value of the stability factor occurs at δ = 0, which is normal to the layers. The minimum value occurs at larger δ values as the dip angle increases, which implies that the steeper the dip angle is, the larger the angle between the possible failure plane and the normal to the layers is. Fig. 8(b) shows that in Model II, the stability factor increases with increasing δ at a given dip angle, which indicates that the most likely failure surface is normal to the layers. Therefore, we mainly concentrate on Model I in the following analysis.

Figs. 9 and 10 show the changes in the lengths of the failure surface in the tensile zone and the shear zone, respectively, with variations in the position of the inter-column force and the slope inclination for a slope height of 17 m and a layer thickness of 0.1 m. The position of the inter-column force has little impact on the length of the failure surface in the tensile zone (Fig. 9); however, it has a significant impact in the shear zone (Fig. 10), and its impact is reduced at high dip angles. In general, l_t decreases with increasing η, and l_s has the opposite pattern.

The distributions of the tensile zone and the shear zone for different dip angles are shown in Fig. 11. Figs. 9–11 show that the length of the failure surface in the tensile zone first increases and then decreases with increasing dip angle, and the length in the shear zone decreases with increasing dip angle. The tensile zone accounts for a larger part of the failure surface than the shear zone, which indicates that the failure mechanism is mainly toppling failure. Fig. 11 also shows that for dip angles larger than 40°, the angle between the failure surface and the horizontal plane is approximately 50°.

Table 2 shows the minimum stability factor, k, as a function of the slope height and dip angle. The impact of the dip angle on the stability factor is the same for slopes with different heigths. The slope stability factor decreases with increasing slope height and dip angle. Furthermore, at dip angles greater than 40°, the angle between the most likely failure surface and the normal to the layers increases with slope height.

Fig. 12 shows the changes in the stability factor and the lengths of the failure surface in the tensile and shear zones in response to changes in the thickness of a single layer for a slope height of 8.5 m and a dip angle of 40°. The relationship between the stability factor, the lengths of the failure surface in the tensile and shear zone, and the thickness of a single layer have the approximate characteristics of logistic curves. The stability factor and length of the failure surface in the shear zone have a positive relationship with the thickness of a single layer, and the length of the failure surface in the tensile zone is negatively correlated with the layer thickness. When the rock layer is thin, the failure mode of the slope is mainly flexural toppling, and it gradually transitions to the

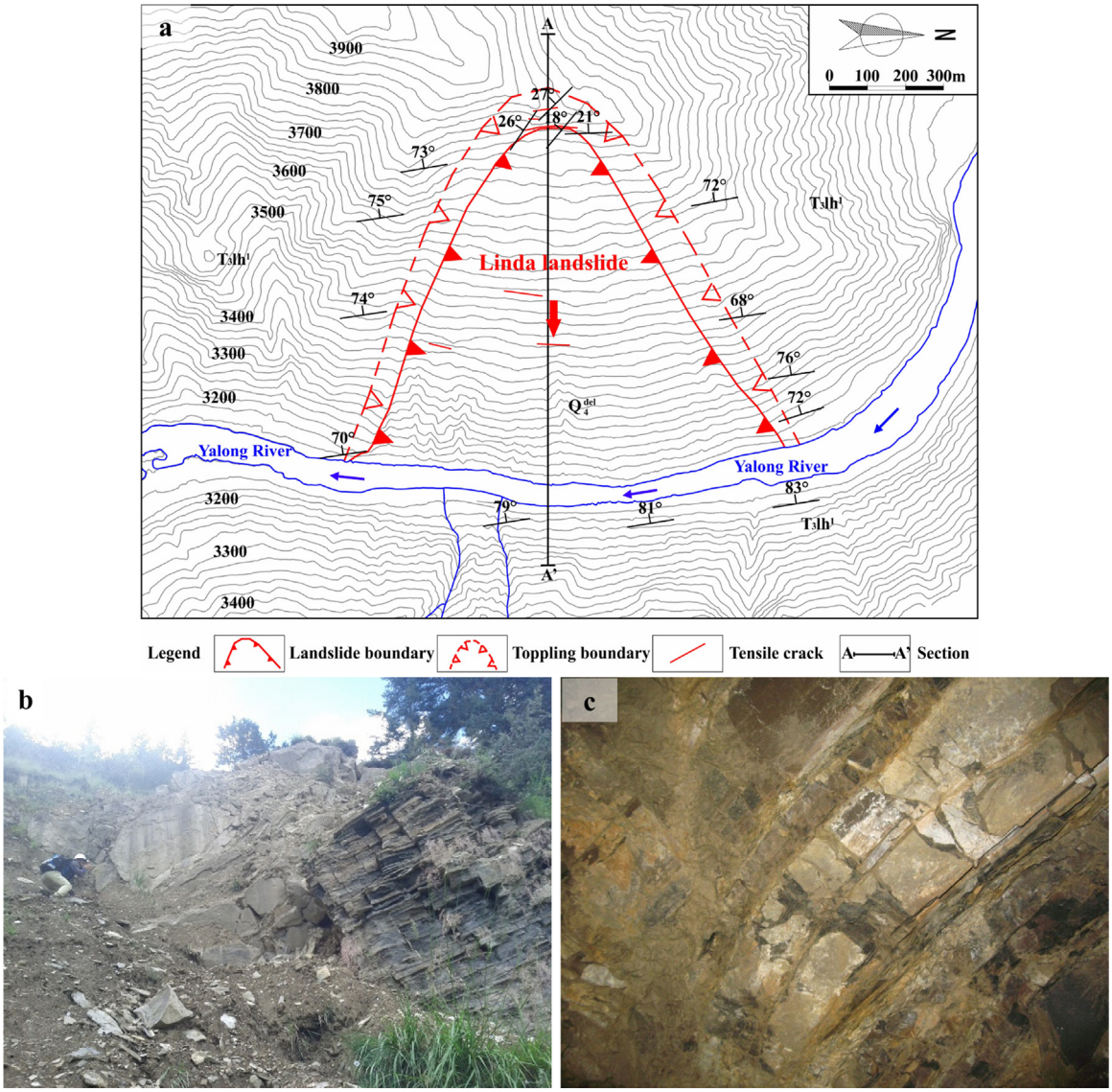

Fig. 13. Linda landslide; a. engineering geological plan of the Linda landslide, b. trailing edge of the landslide, c. strata in the deep of sliding bed.

shear-sliding mode with increasing thickness.

6. Case study

To verify the practicability of the proposed method, a real case study, the Linda landslide (Fig. 13), was selected and analyzed using the Microsoft Excel spreadsheet. The Linda landslide is an ancient landslide located on the right bank of the reservoir region of the proposed Le'an Hydropower Station approximately 5.6–6.8 km from the dam site in the Garzê Tibetan Autonomous Prefecture, Sichuan Province, China. The landslide's trailing edge is located at an elevation of approximately 3,765-3770 m, and the riverbed is at an elevation of 3142 m. The strata of the sliding bed are mainly composed of metasandstone and slate of the Triassic Lianghekou group (T_3lh^1). The beds strike NW15°–25°, which is nearly parallel to the slope , and dip into the slope at approximately 75°. The thickness of the strata vary from 0.2 m to 1.0 m with an average of 0.3 m.

The Linda landslide is a representative case of flexural toppling failure. During its geologic history, the free face of the original slope expanded constantly due to erosion by the Yalong River. Because of gravity, the strata bent downward, and tensile failure occurred. With ongoing bending deformation, the size of the tensile zone increased gradually, and sliding occurred when the shear stress of tensile zone exceeded the shear strength of the rock mass at the toe. Here the proposed method is applied to calculate the stability factor of the anti-dip rock slope before the Linda landslide was formed, which is the key parameter to determine whether or not the landslide happened. Fig. 13(b) shows the trailing edge of the landslide, where the rock mass was bent so intensely that the strata are nearly horizontal. Rocks in the sliding bed were bent intensely at depth as well (Fig. 13(c)). Based on the variation in the dip with depth, the sliding bed is divided into three zones: an area of intense deformation (dip angles < 35°), an area of weak deformation (dip angles 35° − 65°) and a normal area (dip angles > 65°). The Linda landslide slid along the surface rather than along the deep zone of bending. The average thickness of the landslide accumulation is 38–75 m, and the maximum thickness is 98 m.

The geomechanical properties of the rock mass and sliding zone were determined through laboratory tests and back analysis, and the results are shown in Table 1. The calculations were performed in the Microsoft Excel spreadsheet using the trial method, and the stability factor of 0.986 occurred when δ was equal to 16°. The lengths of the failure surface in the tensile zone and the shear zone were also calculated in the Microsoft Excel spreadsheet. Fig. 14 shows the geomechanical model of the landslide with the location of the calculated failure

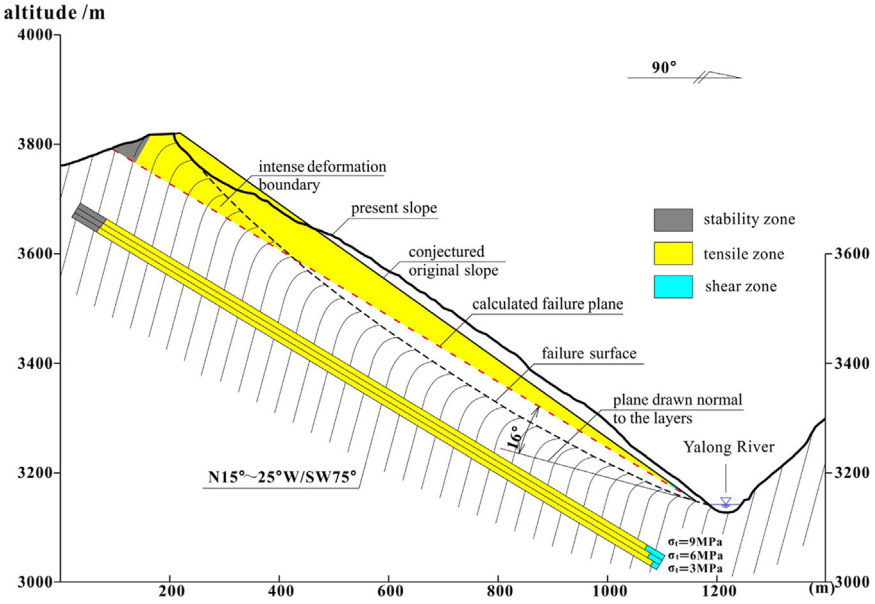

Fig. 14. Failure model of the Linda Landslide calculated using the proposed method (Section A-A′ in Fig. 13(a)).

plane and the ranges of the stability zone, tensile zone and shear zone. The sliding was calculated to occur along the slope surface, and the calculated failure plane was near the sliding surface of the Linda landslide. However, it should be noted that the calculated failure plane was not completely consistent with the actual sliding surface. This was because the proposed method assumes that the failure occurred along a plane, whereas the sliding surface of the Linda landslide was somewhat curved. Fig. 14 also shows that the stability zone was consistent with the actual conditions. The calculated stability factor was less than 1.0, which indicates that the calculated slope was in an unstable condition and is consistent with the fact that the Linda landslide already failed. Based on the results of this case study, the proposed method can accurately calculate the stability factor and failure plane of a flexural toppling failure.

Based on this case study, the changes in the lengths of the failure surface in the tensile zone and shear zone with different shear strengths of the rock mass (9 MPa, 6 MPa, 3 MPa) were studied. The results are shown in Fig. 14 and demonstrate that the shear strength has little effect on the range of the stability zone but has a significant effect on the ranges of the tensile zone and shear zone. The length of the failure surface in the tensile zone increased with increasing shear strength, whereas the length of the failure surface in the shear zone decreased.

7. Conclusions

This paper presented a new method for calculating the stability of rock slopes subject to flexural toppling failure. The flexural toppling failure mode of rock slopes was described as having three steps: the first step is the stability zone, the tensile zone forms next, and the shear zone forms last. This proposed stability method can be used to calculate the stability factor of rock slopes subject to flexural toppling. The ranges of the stability zone, the tensile zone and the shear zone can also be determined. Using this method, analyses of the effects of the position of the inter-column force, the inclination and thickness of the layers, and the height of the slope on the stability factor and the distributions of the tensile zone and the shear zone showed that the position of the inter-column force has almost no effect on the stability factor. In addition, the stability factor of the rock slope decreases gradually with increasing slope height and dip angle and decreasing layer thickness. The angle between the possible failure surface and the normal to the layers increases with increasing dip angle and slope height. Furthermore, the thickness of the layers influences the failure mechanism, which gradually transitions from shear-sliding failure to toppling failure with decreasing layer thickness. Finally, a real case was studied, and the results showed that this method accurately calculates the stability of rock slopes subject to flexural toppling failure.

Acknowledgments

This research is supported by the National Natural Science Foundation of China (Grant no. 41472265).

References

1. Ashby J. *Sliding and Toppling Modes of Failure in Model and Jointed Rock Slopes [Dissertation of Master Degree]*. London: Royal School of Mines; 1971.
2. Goodman RE, Bray JW. Toppling of rock slopes. In: *Proceedings of the ASCE Specialty Conference on Rock Engineering for Foundations and Slopes*, Boulder, Colorado; 2; 1976: 201–234.
3. Cruden DM. Limits to common toppling. *Rev Can De Géotechnique.* 1989;26(4):737–742.
4. Aydan Ö, Shimizu Y, Ichikawa Y. Effective failure modes and stability of slopes in rock mass with two discontinuity sets. *Rock Mech Rock Eng.* 1989;22(3):163–188.
5. Kliche CA. *Rock Slope Stability*. Littleton, CO: Society for Mining, Metallurgy, and Exploration (SME); 1999.
6. Zanbak C. Design charts for rock slopes susceptible to toppling. *J Geotech Eng.* 1983;109(8):1039–1062.
7. Bobet A. Analytical solutions for toppling failure. *Int J Rock Mech Min Sci.* 1999;36(36):971–980.
8. Sagaseta C, Sánchez JM, Cañizal J. A general analytical solution for the required anchor force in rock slopes with toppling failure. *Int J Rock Mech Min Sci.* 2001;38(3):421–435.
9. Liu CH, Jaksa MB, Meyers AG. Improved analytical solution for toppling stability analysis of rock slopes. *Int J Rock Mech Min Sci.* 2008;45(8):1361–1372.
10. Aydan Ö, Kawamoto T. The stability of slopes and underground openings against flexural toppling and their stabilisation. *Rock Mech Rock Eng.* 1992;25(3):143–165.
11. Amini M, Majdi A, Aydan Ö. Stability analysis and the stabilisation of flexural toppling failure. *Rock Mech Rock Eng.* 2009;42(5):751–782.
12. Amini M, Majdi A, Veshadi MA. Stability analysis of rock slopes against block-flexure toppling failure. *Rock Mech Rock Eng.* 2012;45(4):519–532.
13. Tatone BSA, Grasselli G. Rocktopple: a spreadsheet-based program for probabilistic block-toppling analysis. *Comput Geosci.* 2010;36(1):98–114.
14. Bray JW, Goodman RE. The theory of base friction models. *Int J Rock Mech Min Sci Geomech Abstr.* 1981;18(6):453–468.
15. Adhikary DP, Dyskin AV, Jewell RJ. A study of the mechanism of flexural toppling failure of rock slopes. *Rock Mech Rock Eng.* 1997;30(2):75–93.
16. Adhikary DP, Dyskin AV. Modelling of progressive and instantaneous failures of foliated rock slopes. *Rock Mech Rock Eng.* 2007;40(4):349–362.
17. Zhang JH, Chen ZY, Wang XG. Centrifuge modeling of rock slopes susceptible to block toppling. *Rock Mech Rock Eng.* 2007;40(4):363–382.
18. Cundall PA. A computer model for simulating progressive, large-scale movements in

block rock systems. In: *Proceedings of the Symposium of International Society of Rock Mechanics* 1(ii-b); 1971: 11–8.
19. Ishida T, Chigira M, Hibino S. Application of the distinct element method for analysis of toppling observed on a fissured rock slope. *Rock Mech Rock Eng.* 1987;20(4):277–283.
20. Simoneit BRT, Schoell M, Kvenvolden KA, et al. Dem modelling of laboratory tests of block toppling. *Int J Rock Mech Min Sci Geomech Abstr.* 1997;3:506–507.
21. Adachi T, Ohnishi Z, Arai K. Investigation of toppling slope failure At route 305 In Japan. *Int Soc Rock Mech.* 1991.
22. Pritchard MA, Savigny KW. The heather hill landslide: an example of a large scale toppling failure. *Can Geotech J.* 1991;28(3):410–422.
23. Hutchison B, Dugan K, Coulthard M. Analysis of flexural toppling at Australian bulk minerals savage river mine. *Proc.* 2000.
24. Adhikary DP, Dyskin AV, Jewell RJ. Numerical modelling of the flexural deformation of foliated rock slopes. *Int J Rock Mech Min Sci Geomech Abstr.* 1996;33(6):595–606.
25. Adhikary DP, Dyskin AV. A cosserat continuum model for layered materials. *Comput Geotech.* 1997;20(1):15–45.
26. Adhikary DP, Dyskin AV. A continuum model of layered rock masses with non-associative joint plasticity. *Int J Numer Anal Methods Geomech.* 1998;22(4):245–261.
27. Alzo'ubi AK, Martin CD, Cruden DM. Influence of tensile strength on toppling failure in centrifuge tests. *Int J Rock Mech Min Sci.* 2010;47(6):974–982.
28. Amini M, Gholamzadeh M, Khosravi MH. Physical and theoretical modeling of rock slopes against block-flexure toppling failure. *Int J Min Geo-Eng.* 2015;49:155–171.